Validation of large-eddy simulation in a plain asymmetric diffuser

By M. Fatica, H.-J. Kaltenbach[1] AND R. Mittal[2]

Motivation

The main motivation for this study comes from the need to validate wall-resolving LES with the dynamic model in the case of a spatially evolving flow with mild separation.

With the increase in computing power, more complex flow configurations are being investigated by means of three-dimensional, unsteady numerical simulation. The concept of large-eddy simulation (LES), in which resolved and subgrid-scale motions are defined by a spatial filter applied to the Navier Stokes equations, has emerged as a promising tool which complements Reynolds averaged Navier Stokes (RANS) computations. The development of the dynamic SGS-model by Germano *et al.*(1991) was a major advance towards a general model which is applicable to an arbitrary flow and does not need adjustment of model parameters.

An important class of flows which has not been simulated extensively with the LES technique is the pressure driven separation from a smooth surface. Mildly separated flows have always been a challenge for experimentalists as well as modelers.

Experimental research on separated flow physics was hindered by the fact that conventional hot-wire technique is direction insensitive and requires a significant mean flow component to produce reliable measurements. With the increasing use of the LDA technique more data sets of separated flows are becoming available which are suitable for validation purposes. A particularly interesting configuration was investigated recently by Obi *et al.* (1993a, 1993b), using a single-component LDA: a fully developed turbulent flow from a long inlet duct enters a plane, asymmetric diffuser with an opening angle of 10°. The flow separates about half way down the deflected wall, and a separation bubble forms which extends into the straight outlet duct where the flow reattaches.

This flow has several desirable features which make it a good test case for validation of a computational technique such as large-eddy simulation:

a) The flow belongs to the class of 'mild', pressure-driven, separation from a smooth wall. Many technical devices are designed to operate close to these conditions since optimum performance is often achieved when the flow is at the verge of separation.

b) The flow exhibits rich flow physics, such as the combined effect of adverse pressure gradient and curvature near the diffuser inlet and incipient separation and reattachment in the outlet duct.

1 Technische Universitaet Berlin

2 University of Florida

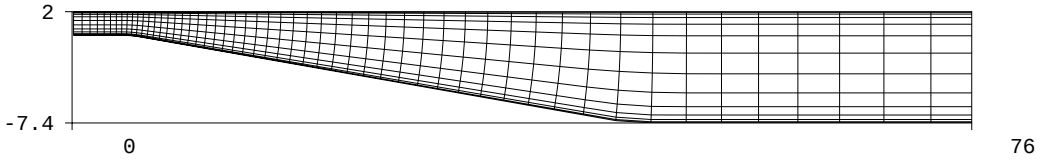

FIGURE 1. Computational domain for the plane diffuser. Only a subset of the actual grid lines is plotted.

c) The inflow conditions are unambiguously defined. The inlet duct has a length of more than 100 duct heights, thereby guaranteeing that the flow entering the expansion is a fully developed turbulent channel flow. For validating the computation of a spatially evolving flow, it is crucial to know the upstream conditions with a high degree of accuracy.

d) The wall-shear based Reynolds number of the incoming channel flow is $Re_\tau = 500$. Although a direct simulation of channel flow is feasible at this value, a DNS of the full diffuser is still prohibitively expensive. The Reynolds number is high enough that the flow does not depend much on this parameter. Obi (1994) did not find significant changes of flow physics when doubling the Reynolds number.

During the course of the work, a closer examination of the experimental dataset from Obi *et al.* (1993a) revealed some inconsistencies. Basic requirements such as mass and momentum balance of the 2D mean flow were not met in the rear part of the expansion (Kaltenbach, 1994). As a result of this, it was felt that an independent confirmation of the experimental data was highly desirable. Therefore, a configuration similar to Obi's rig was built, and great care taken to ensure that the data set satisfied basic requirements for validation purposes (Buice & Eaton, 1996, 1997). For simplicity we refer from now on to the Obi and the Buice experiment, respectively.

Flow configuration

The diffuser geometry as shown in Fig. 1 and Reynolds number $Re_b = U_b\delta/\nu = 9000$ match the experimental configuration of Obi and Buice. Here, the Reynolds number is based on the bulk velocity U_b found in the inlet duct of height $h = 2\delta$. The parallel flow from the inlet duct enters the asymmetric diffuser characterized by an expansion ratio $a = h_{out}/h_{in} = 4.7$ and by an opening angle of 10 degrees. The expanding section extends over 42δ and is followed by a tail-duct of height 9.4δ. With the tail-duct extending over approximately 30δ, the exit plane is located near $x/\delta = 75$. At this location the flow has reattached but is far from being in equilibrium. In the present study we focus on the separation and reattachment and not on the recovery into a canonical channel flow, which occurs over a length of tens of heights of the exit channel.

Simulations were performed on three different meshes and for domain widths of 4δ and 8δ in the spanwise direction. The mesh is stretched in the streamwise and wall-normal direction. Details on the numerical method are given in Fatica & Mittal

(1996).

Computationally, this flow is very challenging because of the large range of timescales encountered. The inertial time scale $\tau = 0.5h(x)/U_b(x)$, based on local diffuser height $h(x)$ and bulk velocity $U_b(x)$, is proportional to the square of the expansion ratio, *i.e.* $\tau_{out} = a^2\tau_{in}$. At the same time, the computational time step is limited by the need to resolve the turbulence in the inlet section. The net effect of the time-scale disparity is that the simulations require very lengthy integration times.

In this brief, we will compare results from two simulations on a domain with a spanwise dimension of 8δ. On the medium mesh ($272 \times 64 \times 96$) the inflow profile has a ratio of centerline to bulk velocity $U_c/U_b = 1.12$, while on the fine mesh ($352 \times 64 \times 128$) the ratio is equal to 1.14, the same value as reported in the experiment of Buice. Before sampling statistics, the simulation is run for an initial period corresponding to approximately one flow-through time in order to flush out the initial transients. Statistics were then sampled over a period of 1080 τ_{in} or 7 flow-through times for the simulation on the medium mesh. The fine simulation is not finished yet and only 3 flow-through times were used. Mean quantities are obtained as averages over both the spanwise direction and time.

Validation of simulation results

The present work aims at exploring the capability of LES for accurate quantitative prediction. For this purpose we compare simulation results with measurements from Obi *et al.* (1993a, 1993b) and Buice & Eaton (1997).

Evaluation of experimental data sets

Meaningful comparison between simulation and experiment hinges on the assumption that the same flow is being studied. Ideally, this requires a match in geometry, inflow and outflow conditions, and Reynolds number. The present state of high-resolution numerical simulations makes it desirable that the computed flows be homogeneous in at least one spatial direction. In a spatially evolving flow such as the diffuser flow, the spanwise direction is considered to be homogeneous. It is hoped that flow physics will become independent of the chosen spanwise domain size once the computational box is wide enough. In this direction periodic boundary conditions can be applied, which is advantageous from a numerical point of view since highly accurate Fourier expansion based methods can be employed. Furthermore, averaging statistics in the homogeneous direction reduces the required sampling time considerably, and this results in significant savings in terms of CPU time.

To set up an experiment of a flow which exhibits spanwise homogeneity remains a challenge. Once the flow separates, the inherent three-dimensionality resulting from side walls of an experimental facility often increases significantly. By choosing configurations with wide aspect ratios, it is hoped that effects from unavoidable secondary flows will be small and will not affect the core region, which should represent a nominally two-dimensional flow.

Assessment of suitability of Obi's data for validation

Obi *et al.* (1993a,b) investigated flow in an asymmetric diffuser using LDA in a wind tunnel. They measured pressure along the flat wall, mean velocity, and Reynolds stresses. The aspect ratio of diffuser inlet and outlet was 1:35 and 1:7.45, respectively. The inlet channel was slightly wider than the diffuser in order to prevent thick sidewall boundary layers from entering the expansion. Buice employed the same technique. In order for the fluid to enter the side slots, the pressure in the slots has to be slightly lower than the ambient pressure. Buice achieved this by obstructing the diffuser exit, thereby raising the average pressure level in the diffuser. Nothing similar is reported for the Obi experiment. Therefore, some doubt remains about the conditions at the diffuser inlet of Obi's setup.

Measurement errors for $\overline{U}$ and Reynolds stresses are estimated to be 0.7% and 2.6% respectively (Maeda *et al.* 1995). Mean flow profiles are two-dimensional within 5% of $\overline{U}$ over 90% of the inlet duct and 60% of the outlet. The mean flow profile measured 22δ upstream of the diffuser throat in the inlet channel is slightly asymmetric. However, the ratio of centerline to bulk velocity at this location is 1.14, which matches closely the prediction by Dean (1978).

The flow-rate per unit width $m = \int \overline{U}(y)\,dy$ computed from profiles measured along the center-plane is plotted in Fig. 2. Up to the end of the expansion near $x/\delta = 40$ the flow-rate is constant within a 2% error band. As the flow leaves the expansion and enters the outlet section the flow-rate increases rapidly. This might indicate that significant secondary flow develops in the outlet section. Obi's data have been made available on ftp-server (Maeda 1995); there, velocity data were scaled in a way such that global mass conservation is guaranteed at every station. We will use the scaled data for comparison with simulation results, keeping in mind that profiles measured downstream of $x/\delta = 40$ should be only used for qualitative comparison.

A special remark is required with respect to proper normalization of pressure measurements which are published in Obi(1993b). There, c_p is given with respect to a reference velocity U_{ref}. Since we choose to present all our data with respect to the bulk velocity of the incoming channel flow, we need to know the ratio U_{ref}/U_{bulk}. Obi *et al.*(1993b) state that the reference velocity corresponds to the centerline velocity of the inlet duct. However, the mean flow profile measured in the inlet duct at $x/\delta = -22$ reaches a peak of $0.975U_{ref}$ (see database of Maeda *et al.* 1995). Thus $U_{ref} = 1.025U_{cent}$, and with $U_{cent}/U_{bulk} = 1.14$, the conversion of c_p given with respect to U_{ref} into c_p with respect to U_{bulk} involves multiplication with the square of $U_{ref}/U_{bulk} = 1.168$. The use of an incorrect reference velocity in Obi (1993b) has been corroborated recently.

Assessment of suitability of Buice's data for validation

The overall dimensions of the experimental facility of Buice (1997) are similar to Obi's setup. The novel feature of this experiment is the fact that the pressure level in the facility was raised through exit blockage, thereby allowing careful control of sidewall boundary layer leakage through slots immediately ahead of the throat. Velocity was measured in air with a hot-wire technique, using single and cross wire

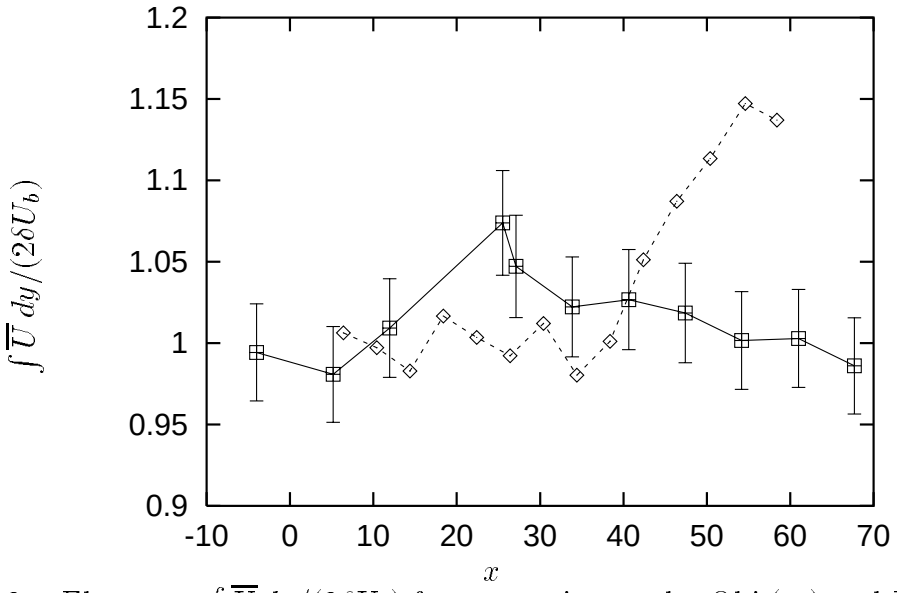

FIGURE 2. Flow rate $\int \overline{U}\, dy/(2\delta U_b)$ from experiments by Obi ($\diamond$) and Buice ($\square$). U_b is the bulk velocity of the inlet channel. Error bars mark 3% deviation.

in regions with significant forward flow and pulsed wires elsewhere. The maximum error in mean velocity is 3%. Flow rates obtained from integration of velocity profiles measured with single wire upstream of separation and a combination of single and pulsed wire elsewhere are plotted in Fig. 2. An increase in flow rate in the order of 5% occurs in the region downstream of $x/\delta = 20$, i.e. immediately behind the zone of maximum pressure rise. Wool tufts mounted to the side walls did not indicate the presence of secondary flow or sidewall separation. The mass-flow deviation in this region is slightly greater than the confidence level for the measurements. No check of spanwise homogeneity at this location is available. Downstream of $x/\delta = 34$ the mass is globally conserved within 3%, and the flow is uniform in the span within 3%.

Force balance

The integral momentum balance for a fixed control volume for the time- and spanwise averaged force component F_x per unit depth is:

$$\sum F_x = (F_{p,out} - F_{p,in}) + F_{p,ramp} + F_{fric} + (F_{visc,in} - F_{visc,out}) = M_{in} - M_{out} \quad .$$

The corresponding control volume consists of vertical cuts at $x_{in} = -4\delta$ and at a downstream position x_{out} and follows the interior of both walls. With α denoting the local angle between the deflected and the horizontal wall, the individual forces read:

$$F_{p,x} = \int_{bot}^{top} \Big(p(x,y) - p_{ref}\Big) dy, \quad F_{p,ramp} = \int_{in}^{out} \Big(p(s) - p_{ref}\Big) \sin\alpha(s) ds \quad ,$$

$$F_{fric} = \int_{in}^{out} \tau_w \cos\alpha(s) ds, \quad F_{visc} = \int_{bot}^{top} \frac{1}{Re}\frac{dU}{dx} dy \ , \quad M_x = \int_{bot}^{top} U^2(x,y) dy \quad .$$

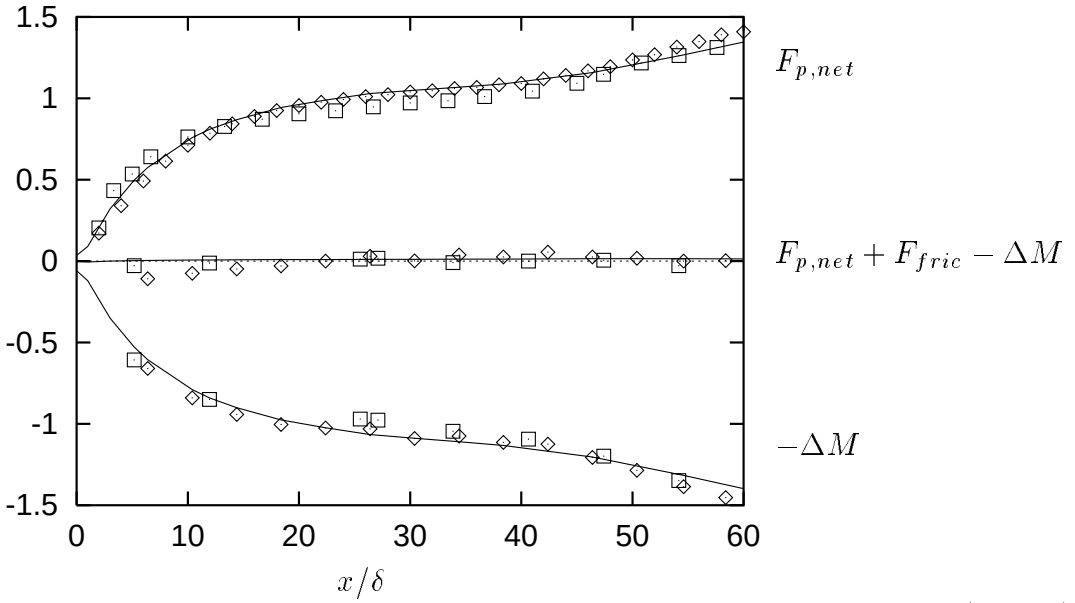

FIGURE 3. Individual terms contributing to the force balance from LES (——), Obi (◇) and Buice (□). Momentum flux difference $-\Delta M = -(M_{in} - M_{out})$ (lower curves), residual $F_{p,net} + F_{fric} - \Delta M$ (middle) and net pressure force $F_{p,net}$ (upper curves) are normalized by δU_b^2.

Here and in the remainder of the brief we set $\rho = 1$. For reference pressure p_{ref} we use the pressure at the lower end of the downstream control volume face. Pressure difference force and ramp force can be combined into a net force $F_{p,net} = F_{p,out} - F_{p,in} + F_{p,ramp}$, which expresses the net effect of pressure acting on all control volume faces. The force $F_{fric,w}$ is evaluated for both walls. The momentum flux M consists of the three parts:

$$M = \int \overline{U}^2 dy + \int \overline{u^2} dy + \int \overline{\tau}_{11} dy \quad .$$

Since the deviatoric SGS-stress τ_{11} is smaller than $2 \times 10^{-5} U_b^2$, it can be neglected in the force balance for LES data. The isotropic part of the SGS stress enters the balance through the pressure. We neglect F_{visc} since the term scales with $1/Re$ and $\partial \overline{U}/\partial x \ll \partial \overline{U}/\partial y$.

Computation of the force balance from experimental data requires some minor modifications such as inserting additional data points near the walls where measurements are scarce and interpolation of c_p-values in x. We assume that the pressure varies linearly across the duct for the experiment. The c_p-difference between wall and interior resulting from the variance $\overline{v^2}$ is on average -0.005 and has been neglected for the experiments. Computing the force balance from LES results using this approximation rather than the real pressure distribution leads to a residual in the order of $0.04 \delta U_b^2$ in the outlet section. The friction force for the experiments is computed using c_f from the LES. Skin friction from the simulation follows closely the measurements of Buice (Fig. 5), and the overall contribution to the momentum

balance is less than 5% of the momentum flux difference between two control volume faces. The overall error introduced by these approximations is assumed to be in the order of 5%.

Figure 3 depicts individual terms and residual of the force balance for both experiments and simulation. The residual is below 1% of the momentum flux difference for LES results, thereby validating the internal consistency of the simulation method and the force balance evaluation. Since friction contributes less than 5% to the momentum balance, the flux difference ΔM is mainly balanced by the net effect of pressure, with $F_{p,ramp}$ contributing about one third of the net pressure force.

The maximum residual for Buice's data set is $0.027\delta U_b^2$, which is below 1.5% of the incoming momentum flux. This accuracy is remarkable considering the approximations involved. We found it to be crucial to use raw data, i.e. velocity measurements which were not scaled to satisfy global mass conservation, in order to obtain a small residual for Buice's data. Obi's data develop a higher residual which exhibits a trend from negative to positive values with streamwise location x/δ. The positive values of the residual might come from neglecting the pressure variation across the duct. Another source for the larger force balance residual compared to Buice's data might be the use of scaled velocity data. Raw data were not available for Obi's experiment.

Although the primary purpose of the force balance is a check of the consistency of experimental data, we have included simulation results in Fig. 3. Since LES and experiment have nearly identical incoming momentum flux, the difference ΔM indicates how much outgoing momentum fluxes differ at the downstream control volume face. LES and Obi's data agree well whereas $M_{x,out}$ is slightly higher for Buice in the region $20 < x/\delta < 30$. Lower ΔM in Buice's data corresponds to a smaller net pressure force downstream of $x/\delta = 20$ compared to simulation and Obi. Note that the enhanced momentum flux is consistent with the slight flow-rate increase in Buice's experiment near $x/\delta = 25$. Since LES and Obi have similar c_p-curves (see Fig. 5), the net pressure force should be close.

Overall, both experimental data sets satisfy mass and momentum balance of a nominally two-dimensional flow within acceptable error bounds, which makes them well suited for validation of a computational study.

Consistency check using Bernoulli's Equation

As a consequence of conservation of energy, the total pressure $c_p + U^2$ remains constant along a stream-tube in an inviscid flow. In Fig. 4, this relation has been evaluated for simulation and experimental data using c_p along the upper wall and the peak value of the streamwise velocity $\overline{U}$ at a given station. Included are data from a RANS computation by Durbin (1994).

Figure 4 reveals that the Bernoulli relation holds only approximately in the diffuser with viscous losses accounting for a 30% decrease over the length of the domain. We find that computations and measurements exhibit about the same total pressure with the exception of Obi's data, which fall short by about 5% of the total pressure upstream of $x/\delta = 15$. We attribute this deviation to the fact that raw data had been scaled to satisfy global mass balance.

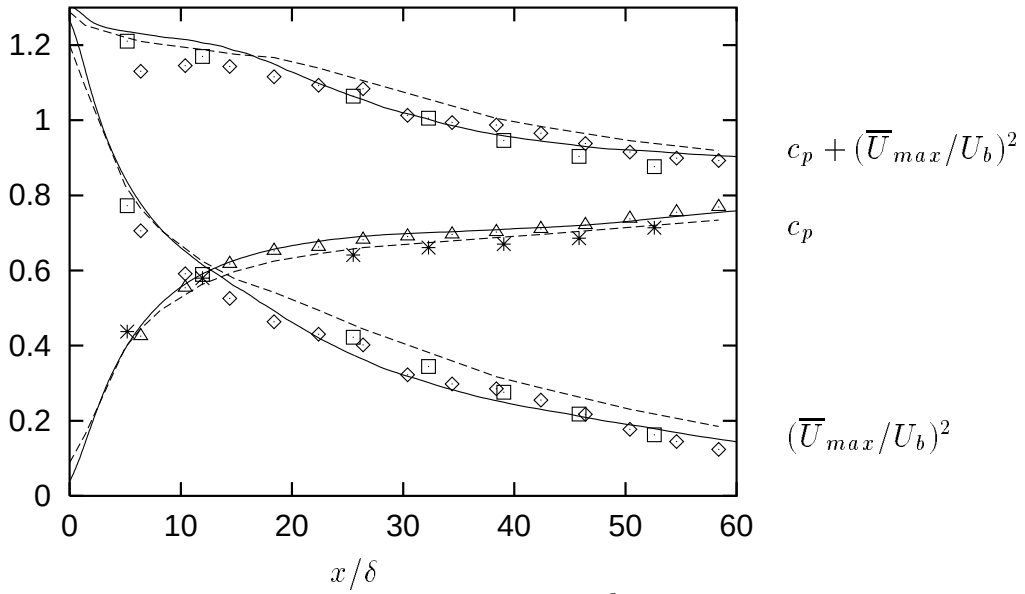

FIGURE 4. Depicted are c_p (lower curves), $\overline{U}^2_{max}$ (middle), and total pressure $c_p + \overline{U}^2_{max}$ (upper curves) normalized by U_b^2 for LES (———), Durbin's RANS simulation (- - - -), and experiments of Obi ($\diamond$, $\triangle$) and Buice ($\square$, *).

Up to $x/\delta = 15$, LES and Durbin's RANS simulation predict larger $\overline{U}_{max}$ than the experiments. However, both cases differ with respect to c_p as early as $x/\delta = 10$. Here, the limitations of the Bernoulli relation for the present configuration become evident. Conversely, the deviation in c_p between LES and Obi on one side and Buice on the other side is consistent with the larger values of $\overline{U}_{max}$ found near $x/\delta = 25$ in Buice's data. There, the flow rate was about 5% higher than in the inlet duct.

Although the Bernoulli relation is only an approximation, it helps to interpret some of the results which will be shown in the following sections. Since the relation between peak velocity $\overline{U}_{max}$ and pressure is quadratic, a seemingly small mismatch in mean flow profile by e.g. 3% translates into a c_p-difference of 6%. This fact highlights the enormous difficulty involved in accurate quantitative prediction of this flow. If through the presence of secondary flow, for example, additional mass flow is added to a given profile which then accumulates in the region where the profile is peaked, even small fractions of the total flow rate are sufficient to increase $\overline{U}_{max}$ considerably, thereby changing the pressure coefficient strongly. It is also evident that error bounds for measurements of $\overline{U}_{max}$ have to be rather small to make data sets useful for validation purposes.

Comparison of LES with experimental data

Using the LES result as a reference, these plots allow comparison of both experiments against each other. From Buice (1997) we use raw data, i.e. data scaled with U_b measured in the inlet duct. Obi's data have been scaled in order to satisfy the global mass balance. One should keep in mind that the uncertainty in the scaling amounts to 15% downstream of $x/\delta = 40$.

Comparison of mean flow and pressure recovery

In Figs. 6 and 7 we compare profiles of mean streamwise velocity $\overline{U}$, rms of velocity fluctuations, and turbulent shear stress $\overline{uv}$ from simulation and experiments. Results from two simulations obtained on different grids are included in these plots. For the validation we restrict ourself to the data from the finest mesh.

Overall, the agreement of mean flow profiles between simulation and experiments is quite good. Upstream of $x/\delta = 10$ the peak velocity $\overline{U}_{max}$ of the simulation is slightly above the experiments. This deviation is within the experimental error margin. Between $x/\delta = 25$ and $x/\delta = 35$ the situation is reversed, i.e. the experiments exhibit slightly higher peak velocities near the flat wall than the simulation. Note that Buice's profiles have not been scaled to conserve mass, which explains the deviation at $x/\delta = 25$ where the flow-rate was 5% high.

The amount of backflow as well as the location and height of the separation bubble agree well up to $x/\delta = 55$. Reattachment and recovery occur further downstream in the simulation as compared to the experiment. This translates into a mean bubble length of 52δ in the simulation compared to 47δ in Buice's experiment. Skin friction along both walls agrees well with Buice's measurements, see Fig. 5. Near the diffuser throat the mean flow detaches over a very short distance, indicated by c_f dropping to zero near $x/\delta = 2$ on the deflected wall. There, a very thin zone of backflow buried in the viscous layer exists that is completely disconnected from the separation bubble, which begins at $x/\delta = 13$ and extends into the tail-duct. Using a thermal tuft, Buice determined the location of vanishing wall stress to be at $x/\delta = 12$. The location of zero crossing in c_f is reached at a shallow angle. Accurate prediction of the exact location of vanishing shear stress is probably less important than of the overall shape of mean flow profiles and the slope of $c_f(x)$.

Most of the pressure increase occurs within the first third of the expansion with the steepest rise close to $x/\delta = 2$ (Fig. 5).

Comparison of Reynolds stresses

Measurement errors are higher for fluctuations as compared to the mean flow, especially at the early stations where measurement volumes are large compared to the local gradients of rms profiles. Buice's measurements of u' are flawed near walls, and the peak rms values are underpredicted by 10-20%. Measurements of v' are available only for regions where the turbulence level remained below 35%. Therefore, only partial profiles are shown in the rear part. A few profiles from the LES upstream of the first measurement stations are shown. The scatter among the two experiments is larger for rms-values and shear stress than for the mean flow. Still, the agreement of the two datasets is good, as can be seen at stations $x/\delta = 27, 34, 38$ where data from both experiments are available.

Rms profiles from all three velocity components exhibit a characteristic shape with a double peak. The location of the peak value moves away from the wall into the flow interior with increasing distance from the diffuser throat. Locations of peaks of all three rms-values are close to each other and coincide with the locations of extremal values of $\overline{uv}$.

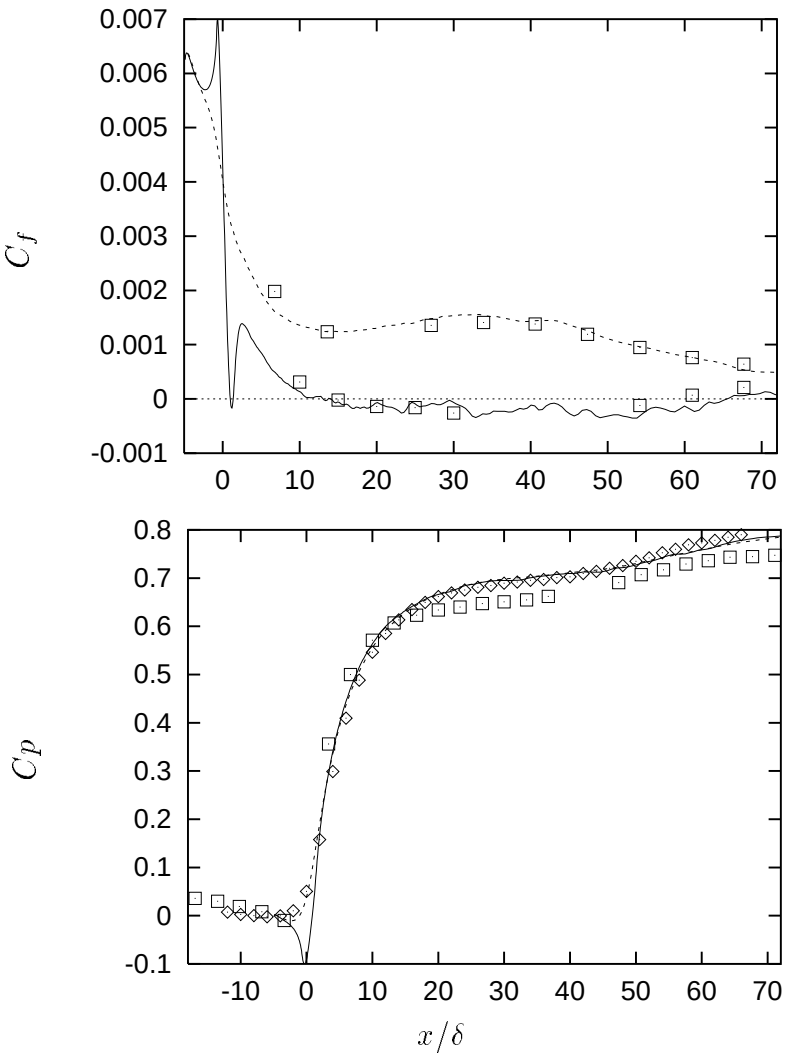

FIGURE 5. Top: Skin friction coefficient c_f based on U_b along deflected wall (———) and flat wall (- - - -) from LES and Buice (□). Bottom: Pressure coefficient c_p based on U_b: LES flat wall (- - - -), LES deflected wall (———), Buice deflected wall (□) and Obi flat wall (◇).

Profiles of u' from the simulation deviate from measurements upstream of $x/\delta = 25$. In this region the peak values of u' on the side of the deflected wall are higher by 10-20% than in the experiments. A similar overshoot is observed for $-\overline{uv}$ in the region $10 < x/\delta < 25$. As mentioned earlier, Buice's measurements for fluctuations have rather large error margins. Inside the outlet section, deviations between simulation and measurements become more pronounced near the separation bubble. Near the flat wall, the agreement for u', v', and $\overline{uv}$ is reasonable. Obi's data are less reliable in this region since the flow is no longer two-dimensional in the mean. The vertical velocity fluctuation v' deviates from measurements downstream of $x/\delta = 12$. There, the part of the v'-profile between flat wall and duct centerline is on average 10-20% higher in the LES than in the experiment. Also, $\overline{uv}$ seems to be higher in this profile section.

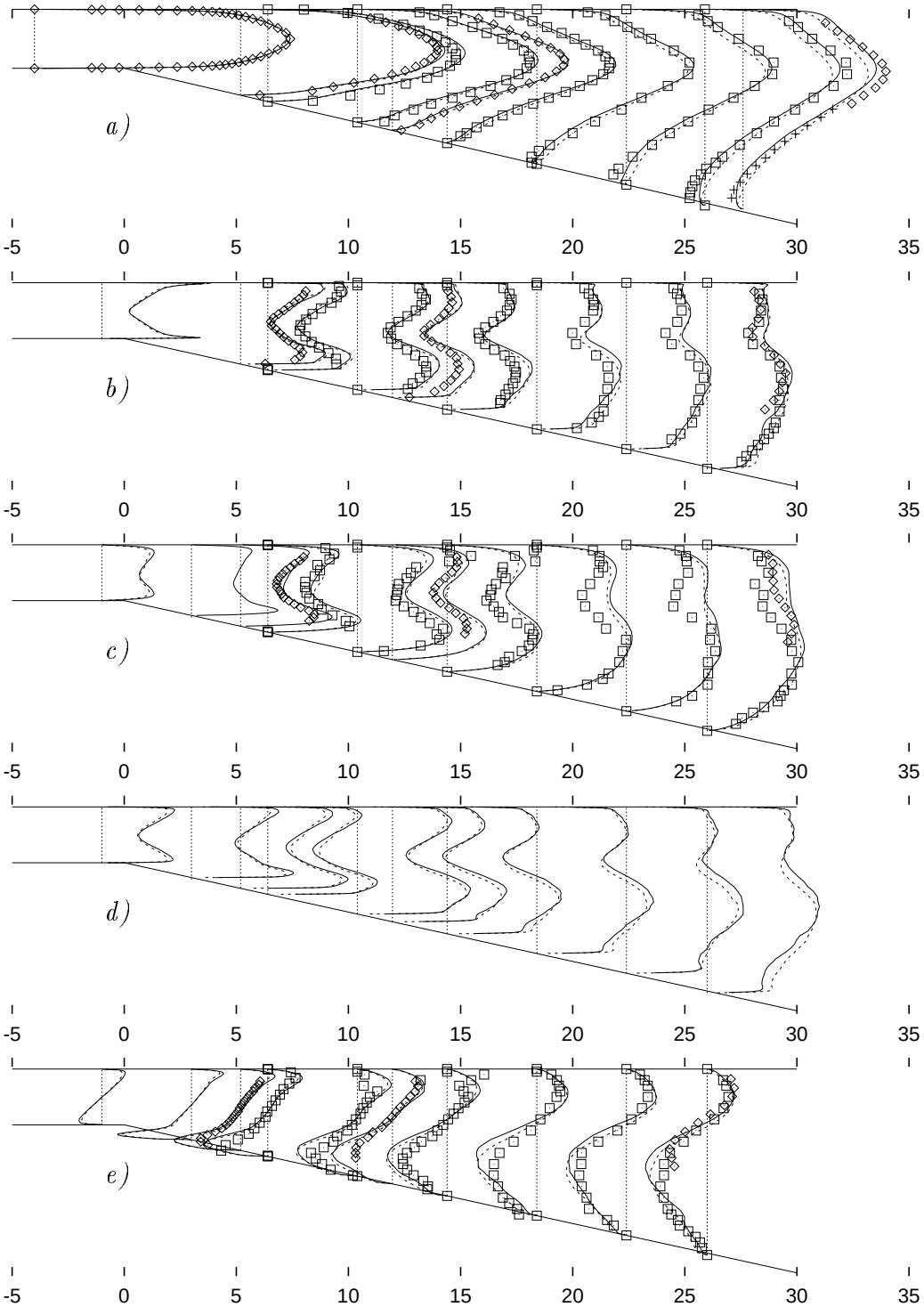

FIGURE 6. Comparison of the LES result on fine (———) and medium (- - - -) grid with data from Buice (□) and Obi (◇), in the first half of the diffuser: *a)* Mean velocity $\overline{U}/U_b$; rms velocity fluctuations: *b)* u'/U_b, *c)* v'/U_b, *d)* w'/U_b, *e)* $\overline{uv}/U_b^2$.

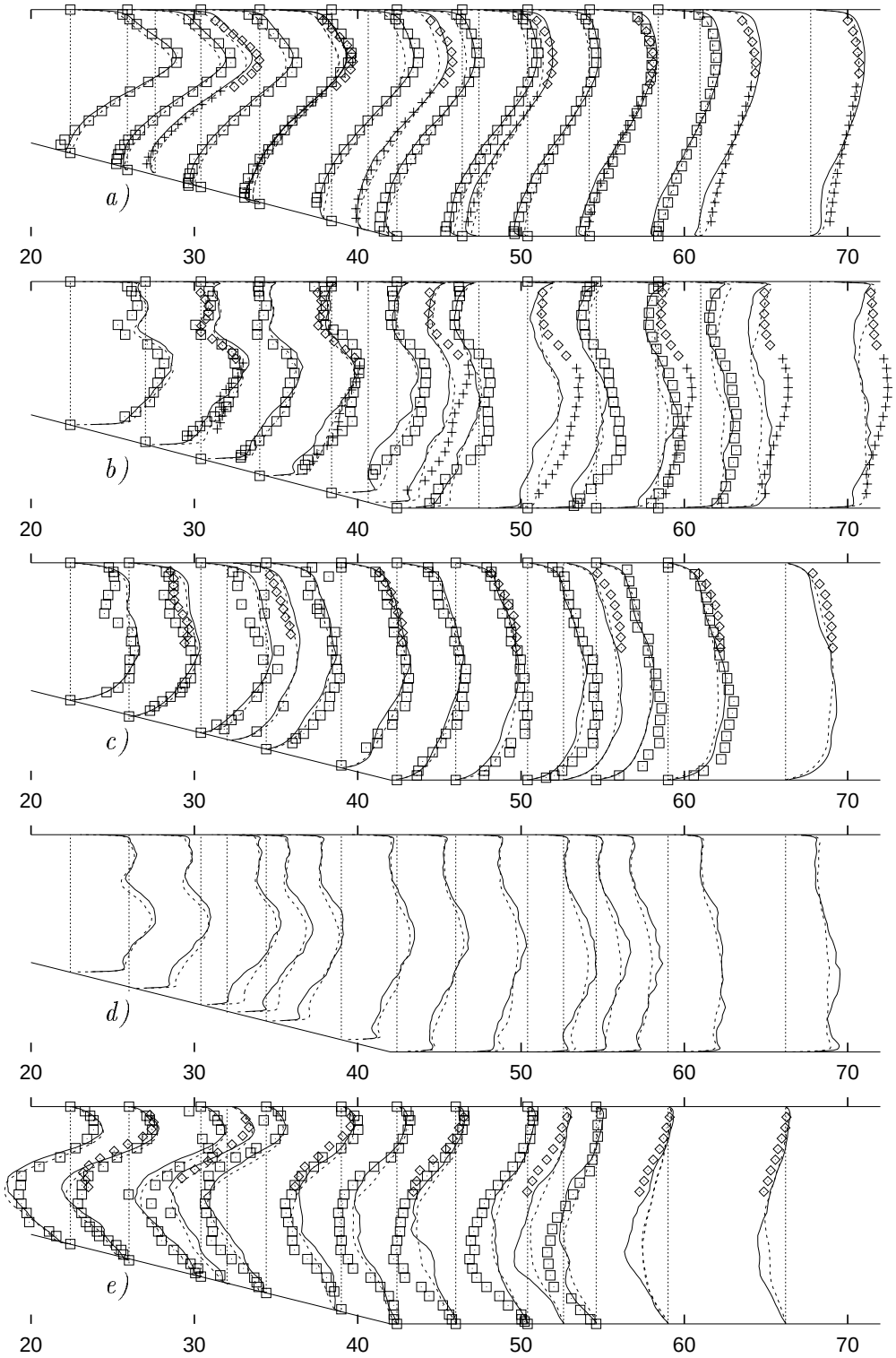

FIGURE 7. Comparison of the LES result on fine (———) and medium (- - - -) grid with data from Buice (□) and Obi (◇), in the rear part of the diffuser: *a)* Mean velocity $\overline{U}/U_b$; rms velocity fluctuations: *b)* u'/U_b, *c)* v'/U_b, *d)* w'/U_b, *e)* $\overline{uv}/U_b^2$.

Conclusion from the validation

Although mean flow and c_p agree well with the measurements, the agreement in Reynolds stresses is not as good. Part of this discrepancy might be due to measurement errors. However, often the deviation of simulation results is outside the scatter of both experimental data sets. It seems unlikely that both experiments suffer from a similar systematic error since different measurement techniques (LDA versus hotwire) were employed.

We find that the simulation captures many essential features of the flow in this configuration, making it a valuable source for a detailed study of the physical phenomena associated with the separation process. With respect to the ability of LES to make accurate quantitative prediction of this flow, some uncertainties remain. Most importantly, it is not clear to what degree the flow in the experiment might be influenced by the presence of secondary flow. A thorough validation requires additional detailed measurements.

Future plans

The simulation on the fine grid is still running, and it will be continued until the statistic are fully converged. In addition, simulations on coarse grids will be performed with interpolated inflow field used for the fine mesh, to investigate the minimal resolution necessary for LES.

Acknowledgments

The simulations were performed at the Numerical Aerodynamic Simulation Facility of NASA Ames Research Center and at the Aeronautical Systems Center under the ASC MRSC Pioneer Program.

REFERENCES

Buice, C. U. & Eaton, J. K. 1996 Experimental investigation of flow through an asymmetric plane diffuser. *CTR Annual Research Briefs-1996,* Center for Turbulence Research, NASA Ames/Stanford Univ. 243-248.

Buice, C. U. & Eaton, J. K. 1997 Experimental investigation of flow through an asymmetric plane diffuser. *Report TSD-107* Dept. of Mech. Eng., Thermosciences Div., Stanford University.

Dean, R. B. 1978 Reynolds number dependence of skin friction and other bulk flow variables in two-dimensional rectangular duct flow. *Trans. ASME I: J. Fluids Engng.* **100,** 215.

Durbin, P. 1994 Separated flow computations with the $k-\epsilon-v^2$ model. *AIAA Journal.* **33,** No. 4.

Fatica, M. & Mittal R. 1996 Progress in the large-eddy simulation of an asymmetric planar diffuser. *CTR Annual Research Briefs 1996,* Center for Turbulence Research, NASA Ames/Stanford Univ. 249-255.

GERMANO, M., PIOMELLI U., MOIN P. & CABOT W. H. 1991 A dynamic subgrid-scale eddy-viscosity model. *Phys. Fluids A* . **3,** 1760-1765.

KALTENBACH, H.-J. 1994 Large-eddy simulation of flow through a plane, asymmetric diffuser. *CTR Annual Research Briefs 1994,* Center for Turbulence Research, NASA Ames/Stanford Univ. 175-184.

MASUDA, S., OBI, S. & AOKI, K. 1994 Control of turbulent separating and reattaching flow by periodic perturbations. *Proceedings of ASME Fluids Engineering Division Summer Meeting Turbulence control, Lake Tahoe, USA.* **FED-Vol. 193,** 55-61.

OBI, S., OHIMUZI, H., AOKI, K. & MASUDA, S. 1993 Turbulent separation control in a plane asymmetric diffuser by periodic perturbation. *Engineering Turbulence Modeling and Experiments 2,* W. Rodi and F. Martelli (Editors), Elsevier Science Publ.

OBI, S., AOKI, K. & MASUDA, S. 1993b Experimental and computational study of turbulent separating flow in an asymmetric plane diffuser. *Ninth Symposium on Turbulent Shear Flows,* Kyoto, Japan, August 16-19, 1993. p.305.